Available online at www.sciencedirect.com
SCIENCE DIRECT®

Journal of the European Ceramic Society 24 (2004) 1121–1127

www.elsevier.com/locate/jeurceramsoc

Application of the differential impedance analysis for investigation of electroceramics

D. Vladikova[a,*], Z. Stoynov[a], M. Viviani[b]

[a]*Central Laboratory of Electrochemical Power Sources-Bulgarian Academy of Sciences, 10 Acad. G. Bonchev St., 1113 Sofia, Bulgaria*
[b]*National Research Council, Institute for Energetics and Interphases, Genoa Department, 6 Via De Marini, 16149 Genova, Italy*

Abstract

This work shows the enhanced performance of Impedance Spectroscopy for investigation and characterization of electroceramics by applying a new structural approach for data analysis, called Differential Impedance Analysis (DIA). The main advantage of this technique is the possibility for model identification directly from the experimental data, i.e. without the use of a preliminary working hypothesis. DIA provides for separation and phenomenological characterization of the different steps involved in the investigated object. The capabilities of the method are demonstrated in conductivity studies of yttrium iron garnet (YIG) single crystal and Er doped PTCR $BaTiO_3$. The analysis ensures a more detailed investigation of the bulk properties of YIG, including the separation and characterization of the hopping conductivity. The application of DIA on $BaTiO_3$ enriches the information about the role of the ferroelectric domain structure on the PTCR.

Keywords: $BaTiO_3$ and titanates; Differential impedance analysis; Electrical conductivity; Ferrites; Ferroelectric properties

1. Introduction

Electrochemical Impedance Spectroscopy is a useful technique for characterization of electroceramic materials. Its principle advantage is that the involved complex process can be extracted from a single measurement, provided a suitable model can be presented as an equivalent circuit. The method ensures separation of the bulk from the grain boundary properties. An important step in this classical data analysis procedure is the model validation, based on the confirmation of the best fit of the equivalent circuit response to the measured data. The procedure follows a statistical approach. Most frequently the complex nonlinear least squares method (CNLS) is applied.[1–5] Its effective use requires the combination of an appropriate equivalent circuit and a set of adequate initial values of the adjustable circuit parameters. In real solid state systems, however, the phenomena are often more complicated than the a priori chosen models and thus the rich information included in the experimental data cannot be fully explored by the standard procedure. Very often the bulk material forms interfaces of new phases, including intergranular porosity. In addition, the optimization of the properties by substitution (doping) may cause the development of vacancy ordered structures. The grain boundaries may be charged, which leads to a depletion or accumulation of space charge in the region adjacent to the interfacial area. Impurities dissolved in the grains or segregated at the grain boundaries, as well as the formation of a new boundary phase, may also influence the impedance behavior. The analysis of experimental impedance diagrams with overlapping depressed semicircles and other complicated shapes needs more sophisticated models with distributed parameters, which cannot be developed a priori on the basis of a preliminary stated working hypothesis. A commonly applied alternative is the introduction of a constant phase element (CPE), which describes frequency distribution.[6] Obviously, the classical approach for data analysis can give a general picture, but it cannot ensure a precise interpretation of the obtained results. A problem solving approach could be sought in the structural modeling, which is widely applied in technical cybernetics. It is more powerful and objective, because it could eliminate the necessity of an initial working hypothesis, extracting the model structure from the experimental data.

Recently, the technique of the Differential Impedance Analysis (DIA), which follows the structural approach, has been developed.[7–10] Its main advantage is the possibility for recognition and characterization of lumped

* Corresponding author. Tel.: +3592-9792765; fax: +3592-722544.
E-mail address: d.vladikova@astratec.net (D. Vladikova).

0955-2219/$ - see front matter © 2003 Elsevier Ltd. All rights reserved.
doi:10.1016/S0955-2219(03)00585-5

or distributed time-constants and dispersed behavior, combined with high selectivity, noise immunity and robustness.[9,10] The results, obtained by DIA, ensure a deeper insight into the investigated objects, providing the observation of new phenomena, which are indistinguishable by standard data analysis. On the other hand, DIA cannot give parametric identification with a very high accuracy.[9] The information obtained for the model structure, however, can serve as a basis for an additional, more precise parametric estimation, based on the CNLS or on other statistical methods.

The DIA technique applies the principle of the scanning local analysis. A simple first order inertial system extended by an additive term, which follows the First Cauer Form,[3] is used as a moving local operating model (LOM). Its structure $\mathbf{S}_{\mathrm{LOM}}$, which gives the model's elements resistances R_1 and R_2 and capacitance C, and their connections, is presented as an equivalent circuit in Fig. 1. The effective time-constant $T = R_2C$ is also regarded as a valuable parameter. The scanning is performed in the whole frequency range with a narrow moving window with a width of few, or even of one frequency point. For each step a parametric identification of the LOM parameters is performed. Obviously the procedure needs a deterministic approach, since statistics cannot be applied in a narrow observation window. For this purpose the initial experimental set of data: frequency ω, real Re and imaginary Im components of the impedance, is extended with the derivatives of Re and Im with respect to the frequency. The LOM parameters' estimates $\hat{\mathbf{P}}(\omega)_{\mathrm{LOM}}$ are obtained by applying the new five dimensional set of data:[7,9,10]

$$\hat{\mathbf{P}}(\omega)_{\mathrm{LOM}} = \mathrm{Par.Ident.}\left[\omega_i, Re_i, Im_i, (\mathrm{d}Re/\mathrm{d}\omega)_i, (\mathrm{dIm}/\mathrm{d}\omega)_i \middle| \mathbf{S}_{\mathrm{LOM}}\right]. \quad (1)$$

The parameters' estimates form a new set of data, which can be written as:

$$\mathbf{D}_{\mathrm{est}}\left[\lg\hat{T}, \lg\hat{R}_1, \lg\hat{\mathrm{C}}, \lg\hat{R}_2\right]. \quad (2)$$

For convenience a logarithmic scale is used. More details for the procedure of the LOM parametric identification can be found in the literature.[7,9,10]

The structure of the investigated object is extracted from the frequency dependence of the LOM parameters' estimates, known as temporal analysis:

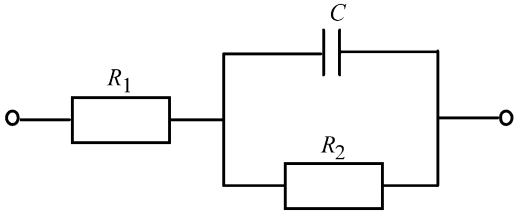

Fig. 1. Equivalent circuit of the local operating model (LOM).

$$\hat{\mathbf{P}}(\omega)_{\mathrm{LOM}} = \mathrm{F}(-\lg f) = \mathrm{F}(\lg T_{\mathrm{f}}), \quad (3)$$

where $T_{\mathrm{f}} = \frac{1}{\mathrm{f}}$ is the period of the sinusoidal signal.

When the object's behavior corresponds to the structure of the LOM in a given frequency range, Eq. (3) shows frequency independence, i.e. this frequency segment of the temporal plot is characterized with a plateau. In the frequency regions where there is no adequacy between the object and the LOM, areas of dispersion appear. They may be due to the mixing of two time-constants, or to the presence of a frequency distributed phenomenon. The next step of the analysis includes the presentation of Eq. (3) in the more informative spectral form. The applied spectral transform technique[7,9,10] represents the plateau from the temporal plot as a spectral line. Its position determines the parameter's estimate, while the intensity corresponds to the frequency range where this estimate has a constant value.

Although developed for recognition of lumped elements, the applied LOM technique can be used for recognition of frequency distribution. In this work special attention is paid to distribution recognition and characterization, since it is important for the investigation of ceramic materials. The application of DIA for impedance investigation of electroceramics is demonstrated in conductivity studies of yttrium iron garnet and barium titanate PTCR ceramics.

2. Experimental

The DIA was performed on two model systems—one with CPE behaviour and one describing a simple time-constant reaction with CPE distributed capacitance, as well as on two electroceramic objects—YIG single crystal and Er doped barium titanate ($BaTiO_3$).

The impedance measurements of YIG single crystal with orientation [110] were performed on a Hewlett Packard 4192A instrument with an amplitude of the a.c. signal 50 mV in a frequency range 13 MHz–1 Hz with a density of 10 points/decade. The experiments were carried out in a temperature interval of 350–650 °C.

The 1 wt.% Er-doped $BaTiO_3$ PTCR ceramics was obtained by the standard ceramic technology. The impedance measurements were carried on a Solartron 1260 FRA with an amplitude of the a.c. signal 1 V in a frequency range 3 MHz–1 Hz with a density of 15 points/decade. The investigated temperature interval was 30–190 °C.

3. Results and discussion

Since CPE is a modelling element, introduced to describe frequency distribution, it cannot be adequate to the applied LOM. The temporal plot of the investigated

CPE, which describes distorted resistance with a CPE exponential coefficient $n=0.1$, has a linear dispersion in the whole frequency range (Fig. 2a). In this case the spectral presentation is not illustrative, because of the lack of an individual spectral line. The linear character of the dispersion, however, suggests the performance of differential temporal analysis as a more emphasizing form of presentation. The projection of the CPE impedance in the differential LOM's space formulates a new set of interdependent functions:

$$\delta_{\hat{R}_2} = \partial \lg \hat{R}_2 / \partial \lg T_f = n, \quad (4)$$

$$\delta_{\hat{C}} = \partial \lg \hat{C} / \partial \lg T_f = n - 1, \quad (5)$$

$$\delta_{\hat{T}} = \partial \lg \hat{T} / \partial \lg T_f = 1. \quad (6)$$

The information contained in Eqs. (4)–(6) can be presented in a spectral form. Since the differential temporal spectra of $\hat{R}_2$, $\hat{C}$ and $\hat{T}$ are interdependent, they may be introduced in one plot, which becomes characteristic for CPE behaviour (Fig. 2b).

The combination of resistance R and capacitance C in parallel formulates a time-constant lumped sub-model, which is the basic mesh for Voigt's model structure,

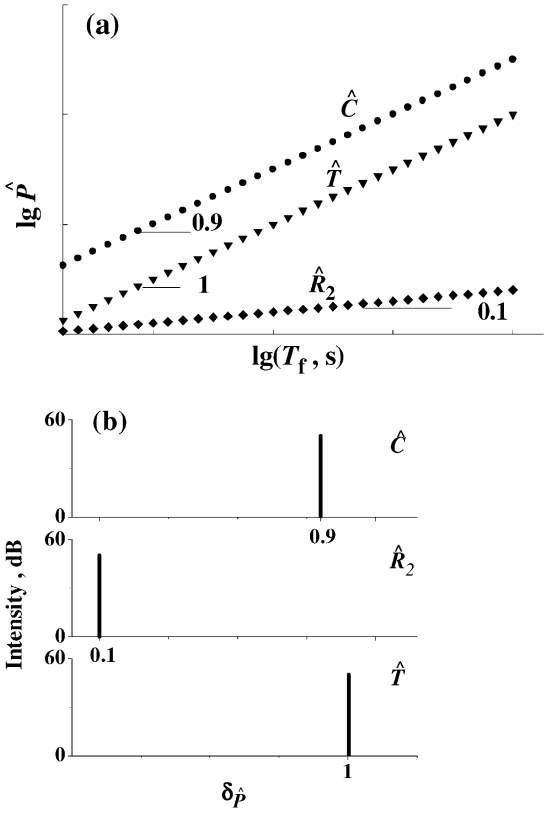

Fig. 2. DIA of CPE with $n=0.1$: (a) temporal plot; (b) differential temporal spectra.

applied in solid state materials studies.[1,3,11] For a better description of the impedance in real systems, where the characteristic semicircles are usually depressed, this sub-model can be generalized by substitution of the capacitance with CPE.[3] Fig. 3 shows the effective $\hat{R}_2$ and $\hat{C}$ temporal plots of the investigated model. Dispersion is observed in both of them, which demonstrates the strong influence of the capacitive CPE on the total impedance behavior of the model. Two quantitative estimations are important for the structural and parametric identification. They are introduced in the $\hat{R}_2$ temporal plot. The high frequency (h.f.) slope in the region before the maximum determines the CPE exponential coefficient, while the value of the maximum gives the effective resistance. The main advantage of DIA in this case is that it can distinguish the depression caused by capacitive CPE from that, which is due to a strong mixing of two time-constants.

YIG is an oxide semiconductor with ferrimagnetic properties. It transforms in the paramagnetic state above the Curie temperature, which is about 260–280 °C. The conductivity of the material is due to the hopping of electrons between the divalent and trivalent iron ions occupying equivalent crystallographic positions.

A typical experimental impedance diagram of the investigated single crystal is presented in Fig. 4a. When the classical approach for identification is applied, a simple time-constant model corresponding to the bulk properties, i.e. to the hopping, is introduced. For a more precise description of the small depression of the semicircle, a capacitive CPE is introduced.

The DIA results are based on the frequency analysis of the LOM parameters R_2 and C. For simplicity in the rest of the text R_2 will be marked with R. The temporal plots obtained (Fig. 4b) can be separated into two frequency segments. In practice the high frequency one (segment I in Fig. 4b) shows no frequency dependence, i.e. it corresponds to the structure of the LOM. This part of the temporal plot is attributed to the hopping conductivity of the material. The low frequency dispersion (segment II in Fig. 4b) can be described with a CPE.

The spectra corresponding to segment I exhibit a well pronounced maximum (Fig. 4c, d). The appearance of fuzzy parts in the $\hat{R}$ spectra is due to the sharper

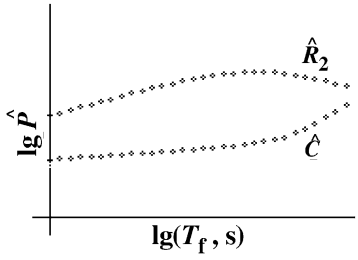

Fig. 3. Temporal plot of a time-constant model with capacitive CPE.

dispersion, observed in the left side of segment I. The spectral images show the lack of temperature dependence of the effective capacitance. The development of $\hat{R}$ spectra with temperature ensures a more precise calculation of the hopping activation energy from the Arrhenius plots, since it eliminates the additional frequency dependent step, described in segment II. The calculated value of about 1.4 eV is higher than that obtained by the classical impedance data analysis with a lumped time-constant model, which is 0.9–1.0 eV.[8]

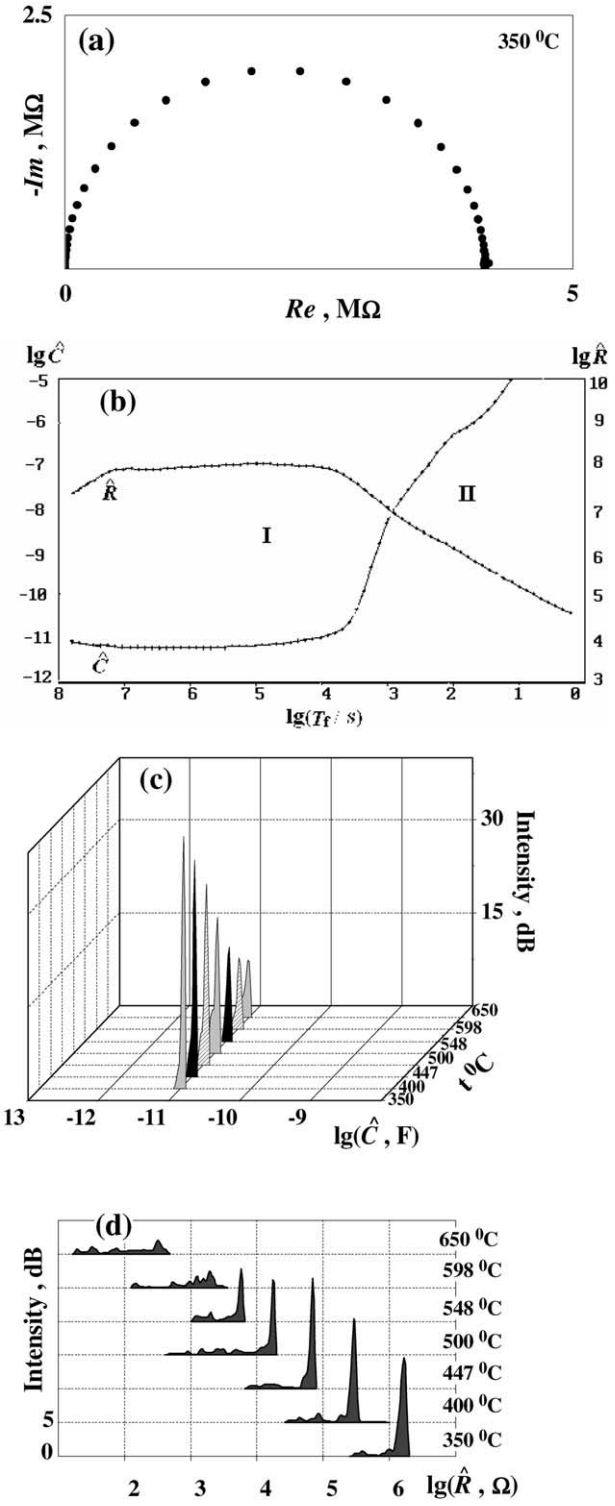

Fig. 4. DIA of YIG: (a) impedance diagram; (b) temporal plot; (c) development of the $\hat{C}$ spectra with temperature; (d) development of the $\hat{R}$ spectra with temperature.

The results obtained show that DIA provides for a more detailed impedance analysis of the bulk properties in YIG, ensuring separation and precise analysis of the hopping conductivity mechanism.

The PTCR of $BaTiO_3$ is connected with the more complicated grain boundary structure, which changes its properties due to a phase transition.[12,13] The description of the system by a two time-constants model with capacitive CPE behavior, is an accepted approximation.[13] However, the existence of a depletion zone in the vicinity of the grain boundaries, combined with a tetragonal ferroelectric domain structure, which transforms with temperature in a paraelectric cubic one, could suppose a priori a more complex behavior, corresponding to different, temperature dependent models.

The temperature development of $\hat{R}$ and $\hat{C}$ temporal plots exhibits a complex behavior, which can be separated in different steps (Figs. 5 and 6). Their number and frequency position change with temperature.

For a deeper analysis of the system, two kinds of segmentation are introduced—temperature and frequency segmentation. The investigated temperature interval is divided into four zones: zone A up to 100 °C (T_{C_1}); zone B 100–130 °C $(T_{C_1} - T_{C_2})$; zone C 130–147 °C $(T_{C_2} - T_{C_3})$; and zone D above 147 °C.

Considering frequency, zones A–C are characterized by two frequency segments—segment I with smooth, quiet behavior and segment II with fuzzy behavior (Fig. 6). In addition segment II is divided in sub-zones IIa and IIb.

The temporal plots corresponding to zone A combine the three frequency segments I, IIa and IIb, which have negligible temperature dependence and very different frequency behavior. The smooth segment I, which shows a slight time-constant frequency dispersion, may be explained by the grain boundary properties of the depletion zone in the tetragonal ferroelectric state of the material. It gives the main contribution to the effective resistance, which slightly decreases with the temperature in this range. Segment I defines the maxima in the spectral plots for zone A (Figs. 7 and 8). The h.f. "tails" in the beginning of Segment I (Fig. 5) suggest the existence of a faster phenomenon, which cannot be observed in the investigated frequency range. It might be attributed to the bulk (hopping) conductivity of the material. This hypothesis needs additional verification.

In our opinion frequency segment II corresponds to the ferroelectric domain structure. Part IIa shows a behavior typical for CPE distribution with decreasing effective resistance and increasing effective capacitance. The frequency dependence in zone IIb is the most

complex one. It cannot be identified with any of the existing impedance elements or models. In addition negative values of $\hat{R}$ and $\hat{C}$ are observed. In principle, the negative resistance and capacitance explain the formation of new phases or substructures, accompanied by energy emission. In the case of ferroelectric $BaTiO_3$ the negative parts of the temporal plots can be explained by reorganization of the domain structure, caused by the a.c. perturbation signal. The fuzzy segments in the low frequency region are an evidence for deviations from the impedance working hypothesis for linearity.[3,14] In this case, however, the observed experimental discrepancy gives additional information about the contribution of the ferroelectric domain structure to the PTCR behavior.

In temperature zone B $(T_{C_1} - T_{C_2})$ continuous and more significant changes, stronger for segment II, occur. Segment I continues to be determining for the effective resistance, which slightly increases with temperature (Figs. 5–7). In the vicinity of T_{C_2} the negative values of the effective capacitance disappear, while the negative $\hat{R}$ shifts towards lower frequencies and vanishes at T_{C_3}. The fuzzy behavior reduces, combined with a shift of IIa to the "right". The temperature development of the temporal plots in zone B suggests hampering of the domain reorganization, due to an increasing domain destruction. At T_{C_2},when the negative segments disappear entirely, the paraelectric behavior is expected to become dominant.

Obviously the lack of ferroelectric polarization above T_{C_2} should increase the grain boundary conductivity barrier and in the interval $(T_{C_2} - T_{C_3})$ (130–147 °C for the investigated composition) the effective resistance, corresponding to the spectral maxima with highest value (Fig. 7), sharply increases (Fig. 9). The frequency segmentation changes not only in behavior, but also in

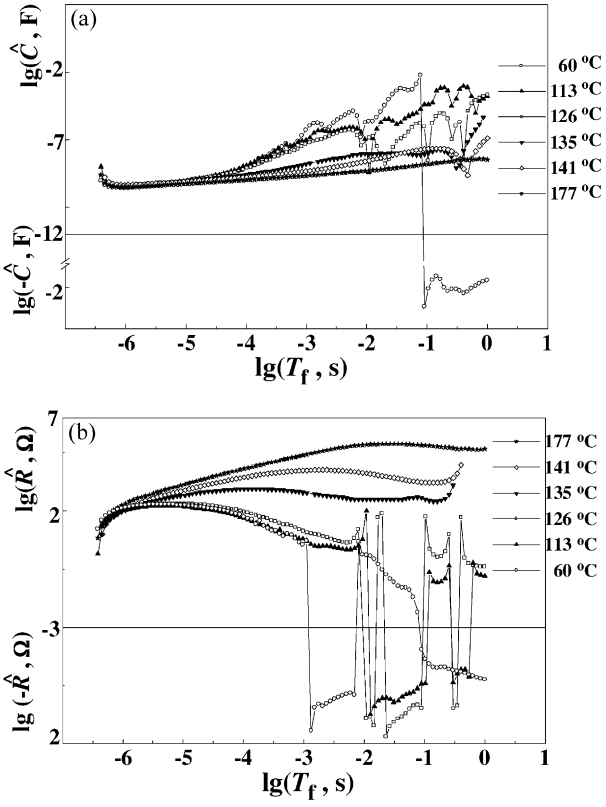

Fig. 5. Development of the temporal plots with temperature for Er-doped $BaTiO_3$: (a) $\hat{C}$ plots; (b) $\hat{R}$ plots.

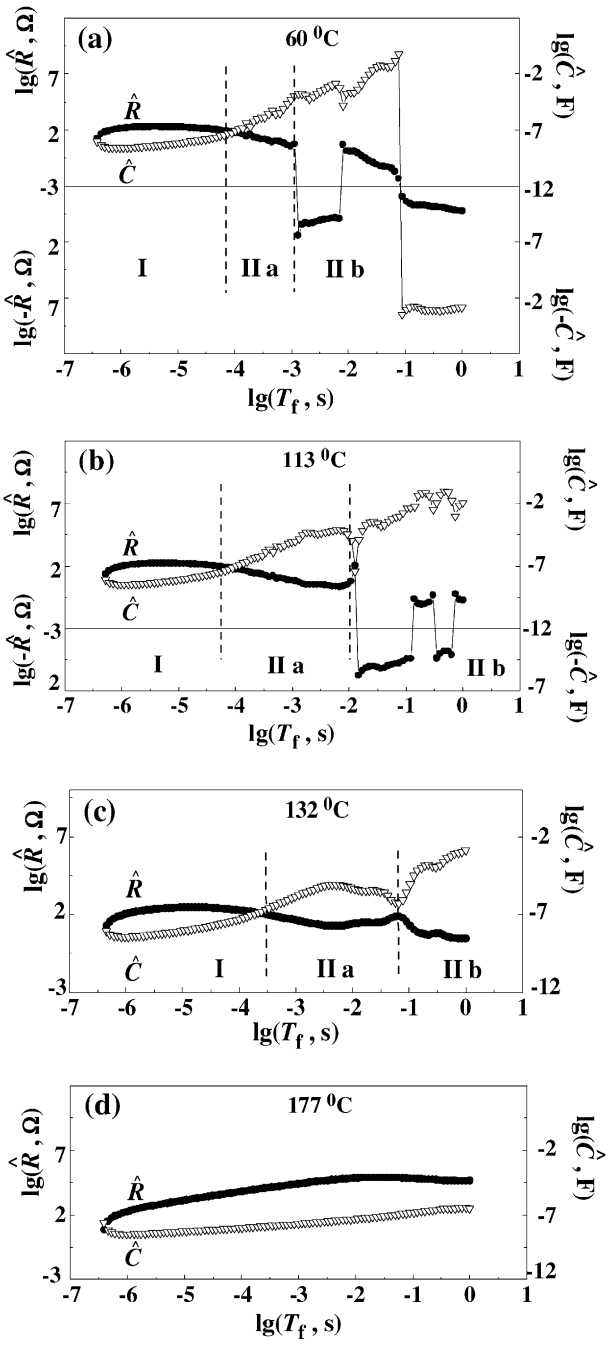

Fig. 6. $\hat{R}$ and $\hat{C}$ temporal plots of Er-doped $BaTiO_3$ at different temperatures.

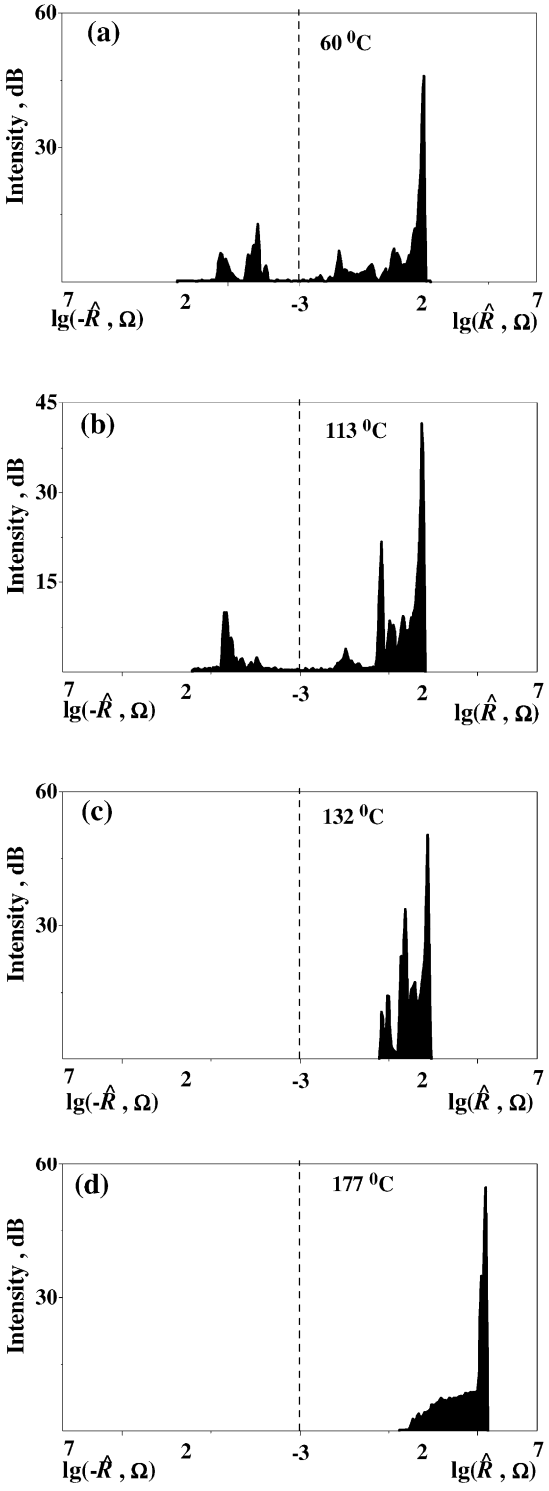

Fig. 7. Development of the $\hat{R}$ spectra with temperature for Er-doped $BaTiO_3$.

the number of steps. In the vicinity of T_{C_2} it transforms in two steps. At T_{C_3} (147 °C) only one frequency distributed step characterizes the whole frequency space. It can be described with the time-constant model with capacitive CPE (Fig. 3).

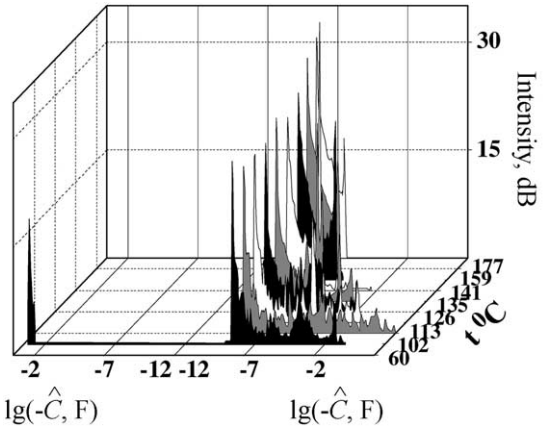

Fig. 8. Development of the $\hat{C}$ spectra with temperature for Er-doped $BaTiO_3$.

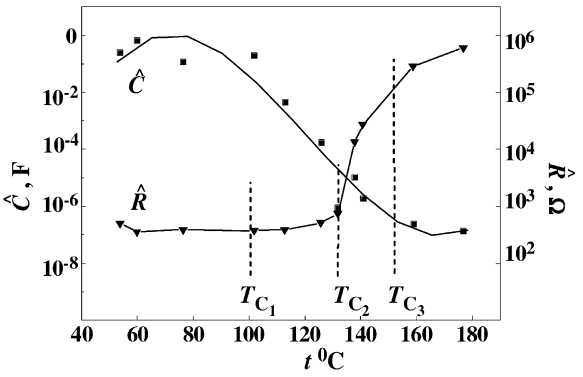

Fig. 9. Development of $\hat{R}$ (obtained by the value of the spectral maximum) and $\hat{C}$ (at a single frequency of 13 Hz) with temperature for Er-doped $BaTiO_3$.

The temperature development of the effective resistance, evaluated by the spectral maxima is shown in Fig. 9. Since the effective capacitance exhibits very strong frequency dependence, its variation with temperature is presented in Fig. 9 for a single frequency (13 Hz).

Our preliminary results for samples with 0.25% Er show similar behavior, characterized again with three critical temperatures $(T_{C_1} - T_{C_3})$, which differ in value.

It could be summarized, that at temperatures under T_{C_1} the PRCR Er doped $BaTiO_3$ has a tetragonal ferroelectric state, which is destroyed progressively in the interval $T_{C_1} - T_{C_2}$. This process is accompanied with a slight increase of the resistance (Fig. 9). In the next critical interval $(T_{C_2} - T_{C_3})$, where the effect of the ferroelectric polarization is negligible, the resistance sharply increases. Above T_{C_3} the material is totally transformed in a cubic paraelectric state.

The application of DIA for description of the PTCR in Er doped $BaTiO_3$ demonstrates the significant influence of the ferroelectric domain structure. The results obtained, which are only the first stage of a more general investigation, confirm the enhanced information

capability of Impedance Spectroscopy, supported by DIA, which overcomes the limitations of the standard modeling.

References

1. Macdonald, J. R., Schooman, J. and Lehnen, A. P., The applicability and power of complex nonlinear least sqaires for the analysis of impedance and admittance data. *Electrochem. Acta*, 1990, **35**, 1483.
2. Boukamp, B. A., A package for impedance/admittance data analysis. *Solid State Ionics*, 1986, **16**, 136.
3. Stoynov, Z., Grafov, B., Savova-Stoynova, B. and Elkin, V., *Electrochemical Impedance*. Publishing House "Nauka", Moscow, 1991.
4. Zoltowski, P., An impedance study of the mechanism of hydrogen reactions on a tungsten carbide electrode. *J. Electroanal. Chem*., 1989, **260**, 269.
5. Lasia, A., Electrochemical impedance spectroscopy and its applications. In *Modern Aspects of Electrochemistry*, ed. B. E. Conway, J. Bockris and R. White. Kluwer Academic/Plenum Publishers, New York, 1999, **32**, pp. 143–248.
6. Sluyters-Rehbach, M., Impedances of electrochemical systems: terminology, nomenclature and representations. *Pure Appl. Chem*., 1994, **66**, 1831.
7. Stoynov, Z., Differential impedance analysis—an insight into the experimental data. *Polish J. Chem*., 1997, **71**, 1204.
8. Vladikova, D., Stoynov, Z. and Ilkov, L., Differential impedance analysis on single crystal and polycrystalline Yttrium Iron Garnet. *Polish J. Chem*., 1997, **71**, 1196.
9. Stoynov, Z., Advanced impedance techniques for lithium batteries study. In *Materials for Lithium-Ion Batteries*, ed. C. Julien and Z. Stoynov. Kluwer Academic Publishers, New York, 2000, pp. 371–380.
10. Vladikova, D., Zoltowski, P., Makowska, E. and Stoynov, Z., Selectivity study of the differential impedance analysis—comparison with the complex non-linear least squares method. *Electrochimica Acta*, 2002, **47**, 2943.
11. Bonanos, N., Steele, B. C. H., Johnson, W. B., Wayne, L. L., Macdonald, D. D. and McKubre, M. C. H., Applications of impedance spectroscopy. In *Impedance Spectroscopy—Emphasizing Solid Materials and Systems*, ed. J. R. Macdonald. Wiley-Interscience, New York, 1987, pp. 191–238.
12. Amin, A. and Newnham, R. E., Thermistors. *Key Engineering Materials, 66&67*, 1992, 339.
13. Viviani, M., Buscaglia, M. T., Buscaglia, V., Mitoseriu, L., Testino, A. and Nanni, P., Electrical properties of Er-doped $BaTiO_3$ ceramics for PTCR applications, In *Proceedings of ISAF XIII 2002*, in press.
14. Gabrielli, C., Identification of electrochemical process by frequency response analysis. Monograph Reference 004/83, Solartron Instr. Group, Farnsborough, England, 1980.